UNIVERSITY OF LEEDS

This is a repository copy of *A census of post-AGB stars in Gaia DR3: evidence for a substantial population of Galactic post-RGB stars*.

White Rose Research Online URL for this paper:
https://eprints.whiterose.ac.uk/193199/

Version: Accepted Version

Article:

Oudmaijer, RD, Jones, ERM and Vioque, M (2022) A census of post-AGB stars in Gaia DR3: evidence for a substantial population of Galactic post-RGB stars. Monthly Notices of the Royal Astronomical Society: Letters, 516 (1). L61-L65. ISSN 1745-3925

https://doi.org/10.1093/mnrasl/slac088

© 2022 The Author(s) Published by Oxford University Press on behalf of Royal Astronomical Society. This is an author produced version of an article published in Monthly Notices of the Royal Astronomical Society: Letters. Uploaded in accordance with the publisher's self-archiving policy.

Reuse
Items deposited in White Rose Research Online are protected by copyright, with all rights reserved unless indicated otherwise. They may be downloaded and/or printed for private study, or other acts as permitted by national copyright laws. The publisher or other rights holders may allow further reproduction and re-use of the full text version. This is indicated by the licence information on the White Rose Research Online record for the item.

Takedown
If you consider content in White Rose Research Online to be in breach of UK law, please notify us by emailing eprints@whiterose.ac.uk including the URL of the record and the reason for the withdrawal request.

White Rose
university consortium
Universities of Leeds, Sheffield & York

eprints@whiterose.ac.uk
https://eprints.whiterose.ac.uk/

A census of Post-AGB stars in Gaia DR3: evidence for a substantial population of Galactic post-*RGB* stars

René D. Oudmaijer,[1]* Emma R. M. Jones,[1] and Miguel Vioque[2,3]
[1] *School of Physics & Astronomy, University of Leeds, Woodhouse Lane, LS2 9JT, Leeds, UK*
[2] *Joint ALMA Observatory, Alonso de Córdova 3107, Vitacura 763-0355, Santiago, Chile*
[3] *National Radio Astronomy Observatory, 520 Edgemont Road, Charlottesville, VA 22903, USA*

Accepted for publication in MNRAS Letters, 2022 July 31.

ABSTRACT

This paper presents the first census of Galactic post-Asymptotic Giant Branch stars in the HR diagram. We combined Gaia DR3 parallax-based distances with extinction corrected integrated fluxes, and derived luminosities for a sample of 185 stars that had been proposed to be post-AGB stars in the literature. The luminosities allow us to create an HR diagram containing the largest number of post-AGB candidate objects to date. A significant fraction of the objects fall outside the typical luminosity range as covered by theoretical evolutionary post-AGB tracks as well as observed for Planetary Nebula central stars. These include massive evolved supergiants and lower luminosity objects. Here we highlight the fact that one third of the post-AGB candidates is underluminous and we identify these with the recently recognised class of post-Red Giant Branch objects thought to be the result of binary evolution.

Key words: stars: AGB and post-AGB — stars: evolution — parallaxes

1 INTRODUCTION

Prior to its final fate as a cooling White Dwarf, the Sun will be going through the Planetary Nebula (PN) phase after having moved from the Asymptotic Giant Branch (AGB) through the subsequent post-AGB (or pre-PN) stage. This scenario is believed to apply to most low- to intermediate mass stars (van Winckel 2003). During the post-AGB phase, the star moves rapidly to the blue in the HR diagram. The phase is typically assumed to end when the central star has reached a surface temperature of 30,000 K, when the star can ionise its envelope and the object appears as a Planetary Nebula. Post-AGB evolutionary timescales depend on the stars' initial masses, and vary from ∼5000 to ∼200 years for stars with initial masses of 1 $M_\odot$ and 4 $M_\odot$ respectively (Schönberner 1983; Blöcker 1995). These are likely upper limits, as, for example, increased post-AGB mass loss rates shorten the transition (van Hoof et al. 1997; Miller Bertolami 2019).

These timescales are extremely short which has hampered the search and identification of post-AGB candidate stars, and their identification came relatively late. AFGL 2688 and AFGL 618 were among the first to be identified as such. Their then newly discovered infrared excess emission due to circumstellar dust betrayed a previous mass losing evolutionary phase (Ney et al. 1975; Westbrook et al. 1975). Much progress has been made since and many more post-AGB candidates stars have been identified and proposed. Of note are the compilations by Suárez et al. (2006) and the Toruń catalogue by Szczerba et al. (2007).

A crucial parameter to parameterise the objects and to place them in an evolutionary context is their luminosity. As the evolution from the AGB to the PN stage occurs more-or-less horizontally in the Hertzsprung-Russell (HR) diagram, the luminosity immediately sets the stars' birth mass, core mass and evolutionary age. Distances have been hard to come by however. A general approach has been to assume a fixed luminosity for all objects, and use the observed integrated flux to then derive the distance. This was the fundamental approach in the first distance catalogue of post-AGB stars published by Vickers et al. (2015). These authors grouped the known post-AGB candidates into subpopulations which were assigned luminosities between 3,500 and 10,000 $L_\odot$. The distance was then determined using the ratio of this luminosity and the total integrated flux which they derived from the stars' Spectral Energy Distributions (SEDs).

With the advent of the Gaia satellite (Gaia Collaboration et al. 2016, 2021) the time is ripe to collate the best available distances for post-AGB stars, determine their luminosities and, where possible, position them in the HR-diagram. Hrivnak et al. (2020) presented Gaia DR2-derived distances for 12 objects, Parthasarathy et al. (2020) presented data for a further 8 objects, while in a recent paper, Kamath et al. (2022) study 31 Galactic post-AGB stars and their Gaia DR3 data. However, a global analysis is yet to appear. Here we make use of the fact that Vickers et al. (2015) derived integrated fluxes for 350 post-AGB stars. In this paper, we derive distances and luminosities for those objects that are present in the Gaia DR3 release and investigate their properties. This results in the most complete census of Galactic post-AGB stars to date.

---

* E-mail: r.d.oudmaijer@leeds.ac.uk

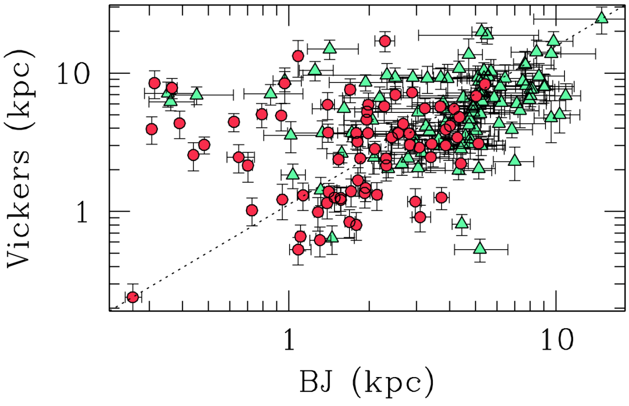

Figure 1. The Bailer-Jones distances for the 185 objects with good parallaxes versus the Vickers distances. Stars with the best parallaxes ($\varpi/\sigma_\varpi > 10$) are denoted by the circles, those with $1 < \varpi/\sigma_\varpi < 10$ by the triangles. The correlation coefficient (in log-space) is 0.37. The dashed line represents the $x = y$ line.

2 SAMPLE SELECTION AND DATA

We draw the sample from Vickers et al. (2015). They determined the integrated fluxes in a homogeneous manner for 209 "likely" and 87 "possible" post-AGB stars from the Toruń catalogue by Szczerba et al. (2007), an additional 54 "miscellaneous" objects were suggested after that catalogue's publication. Vickers et al. (2015) determined the total integrated flux through fitting multiple black body functions to the SED for all 350 objects, after de-reddening the spectral energy distributions (SED) using interstellar extinction values presented by Schlafly and Finkbeiner (2011) and Arenou et al. (1992). Although this approach does not account for circumstellar reddening, it is to first order a good approximation as the re-emitted energy in the infrared is captured fully by the SED in case of spherical shells, while the approach was homogeneously applied to the entire sample. The uncertainties on the fluxes listed by Vickers et al. (2015) are typically 20%.

150 of the 209 "likely", 62/87 "possible" and 37/54 miscellaneous post-AGB stars (so 249/350 in total) have Gaia DR3 parallaxes (Gaia Collaboration et al. 2021). Distances based on parallax data can be determined in various ways, for high quality parallaxes it can be straightforwardly determined by inverting the parallax. For less well determined parallaxes, the larger errorbars result in notably a-symmetric errors once inverted and an accurate distance determination based on a simple inversion proves not possible. This can be alleviated by assuming an *a priori* distribution of stars in the Milky Way; Bailer-Jones et al. (2021) used a Bayesian approach to obtain new distance estimates based on Gaia DR3 parallaxes. Two sets of distances were returned by Bailer-Jones et al. for DR3, the geometric distances which were solely based on the astrometry and the photometric distances which were additionally based on the stellar magnitudes and colours. As the latter method makes implicit assumptions about the nature of the objects, we proceed with the geometric distances. For objects which have $\varpi/\sigma_\varpi < 1$ or even a negative parallax, the Bailer-Jones values tend to converge to the prior, and distances thus derived are arguably not very useful.

249 out of the 350 Vickers post-AGB candidates have a DR3 parallax. Of those, 74 have very well determined parallaxes ($\varpi/\sigma_\varpi > 10$), 111 have good parallaxes ($1 < \varpi/\sigma_\varpi < 10$), while the remaining 64 objects have poorly determined parallaxes with $\varpi/\sigma_\varpi < 1$. We will continue in the following with the 185 objects with good parallaxes and use the Bailer-Jones distances throughout. We note that the inverted parallaxes and Bailer-Jones distances are almost identical for the highest quality parallaxes.

2.1 Comparison with the Vickers distance catalogue

It is an interesting exercise to see the impact Gaia has on our knowledge of post-AGB stars and their evolution. As noted above, distances of these objects were hard to come by and Vickers et al. (2015) produced the largest and arguably best distance catalogue for post-AGB stars at the time. Fig. 1 shows the Vickers distances against the Gaia-based distances. It appears there is hardly a correlation and indeed, a correlation coefficient of 0.37 is returned. Many objects are, often significantly, closer than the Vickers distances. This means that their Gaia-based luminosities are much lower than originally assumed. We are forced to conclude that the pre-Gaia distances were not a good indication of the true situation. This can in part be due to the underlying assumption that the objects are post-AGB stars. If they are not, then the originally assumed post-AGB luminosity would be wrong to begin with. We return to this notion later.

3 RESULTS

3.1 The HR Diagram

In order to place the objects in an HR-diagram, we need both the luminosities of the objects and their temperature. The stellar luminosities are computed by multiplying the, dereddened, integrated fluxes (in terms of luminosity per kiloparsec squared) from Vickers et al. (2015) with the square of the Gaia-based distance (in kpc). Regarding the temperatures, we found spectral types for 167/249 objects, the vast majority of those were sourced from the SIMBAD database. For the spectral type to temperature conversion, we consulted the tables by Straizys and Kuriliene (1981). As we will use the HR diagram only for illustrative purposes in this paper, we do not need precise temperatures.

The resulting HR diagram is shown in Fig. 2 which contains the 134 post-AGB stars for which we have both Gaia-based distances and temperatures based on the spectral types. For reference, the post-AGB evolutionary tracks (Miller Bertolami 2016) are plotted. The core masses of the tracks range from 0.528 $M_\odot$, corresponding an initial mass of 1 $M_\odot$, to a track for 0.833 $M_\odot$, corresponding to stars with an initial mass of 4 $M_\odot$. These tracks encompass the bulk of the objects that would be observable in their post-AGB phase at present; not many stars in the Galaxy with initial masses lower than 1 $M_\odot$ will have evolved through the post-AGB phase, while their crossing times become so long that their circumstellar material will have long dispersed into the interstellar medium. Objects with initial masses of 4 $M_\odot$ have a post-AGB crossing time less than 100 years, a timescale that rapidly decreases with initial mass. There are not many high mass objects in general, but given the shorter timescales, few higher mass objects will be observable as a post-AGB star.

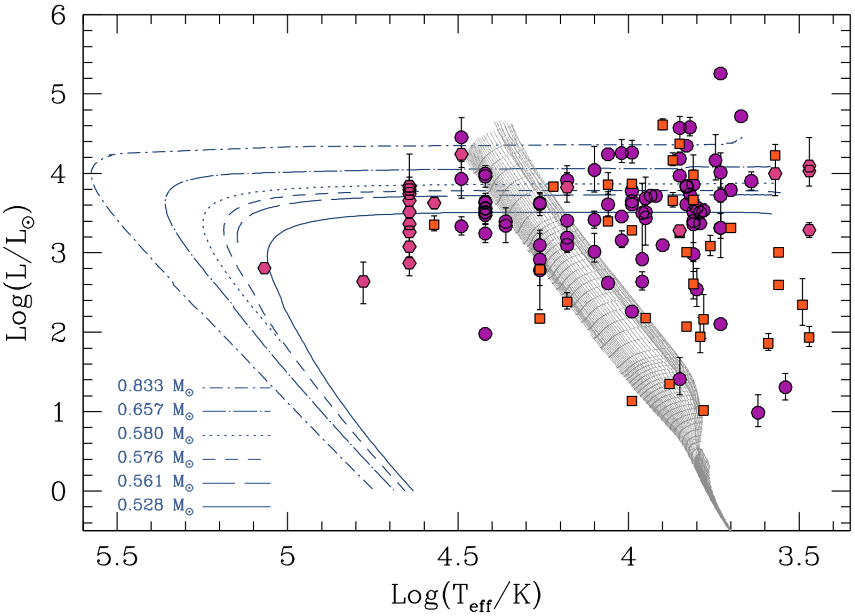

Figure 2. HR diagram of the 134 post-AGB objects with both Gaia-based distances and temperature information available. The post-AGB evolutionary tracks are taken from Miller Bertolami (2016) and computed for solar metallicity. The (core) masses are indicated in the bottom left, and correspond to intial masses from 1 - 4 $M_\odot$. The Main Sequence is taken from the PARSEC tracks (Bressan et al. 2012). The "likely" post-AGB objects are denoted by the purple circles, the "possible" objects as filled orange squares and the "miscellaneous" post-AGB stars are represented by pink hexagons. The object classifications are those from Vickers et al. (2015).

Most post-AGB candidate stars are indeed located along the theoretical evolutionary tracks. However, many objects, including some with the smallest distance uncertainties, are located outside these most extreme tracks, both above (up to more than 10^5 $L_\odot$) and below (as low at 10 $L_\odot$) the lines. We recall that the HR diagram only contains a sub-sample of objects, namely those with spectral types, allowing their positioning in the HR diagram. Let us now investigate the fuller sample of 185 objects with Gaia-based luminosities.

3.2 The luminosities of post-AGB star candidates

Fig. 3 shows a histogram of the luminosity of the objects from the "likely", "possible" and "miscellaneous" categories and the total sample. All groups peak in the lower end of the luminosity range for post-AGB stars. Using the mass-luminosity relationship by Herwig et al. (1998), the peak luminosity translates into a mass that agrees with the observed peak mass of White Dwarf stars of 0.562 $M_\odot$ reported by Bergeron et al. (1992) and which corresponds to ∼4665 $L_\odot$. The values also agree with those observed for Planetary Nebula central stars before they enter the cooling track (González-Santamaría et al. 2021, based on Gaia data).

However, the luminosities span a wide range from 10 to several 10^5 $L_\odot$. A significant fraction of the objects falls outside the Miller Bertolami (2016) post-AGB tracks for stars with initial masses of 1 - 4 $M_\odot$ respectively. The two brightest objects are found to be IRAS 17163-3907, the central star of the Fried Egg nebula and HD 179821. Both are known massive evolved stars in their post-Red Supergiant phase (Koumpia et al. 2020; Oudmaijer et al. 2009) and due to their similarity with post-AGB stars had often been included in such samples. Yet, the large number of underluminous objects is arguably the main eye-catching finding. These will be discussed below.

4 DISCUSSION

We combined Gaia DR3 data with extinction corrected integrated fluxes, and derived luminosities for a large sample of objects that have been proposed to be post-AGB stars in the literature. Most objects have luminosities as expected for the class, yet many appear to be underluminous. Before discussing their nature, let us first investigate whether any observational effects have affected the results.

The luminosity determination: The main errors on the luminosity determination are due to uncertainties in the distance and the flux determination for the objects themselves. To start with the former, the histogram bin sizes in Fig. 3 are larger than the errors on the stars' luminosities, while it can also be seen in the HR diagram that objects with the smallest errors on the luminosity are clearly below the canonical post-AGB tracks, strongly suggesting the observational uncertainties do not bias the results.

Another uncertainty entering the computation of the luminosity is that of the determination of the total integrated flux. Vickers et al. (2015) report that the errors on their flux determination are of order 20%. As a check on the accuracy of these authors' global approach, we compare the total integrated fluxes as derived by them with the 31 objects published in Kamath et al. (2022). The latter authors took into account the total extinction using known stellar parameters in contrast to Vickers et al. (2015) who only took into account interstellar extinction as outlined earlier. The literature val-

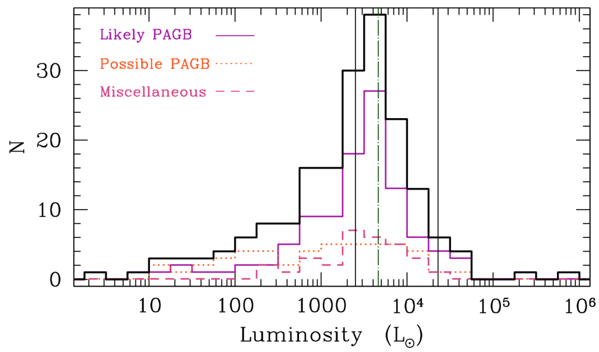

Figure 3. The Gaia-based luminosities of 185 post-AGB objects for the various categories of post-AGB star as listed by Vickers et al. (2015), and the total. The solid vertical lines correspond to luminosities for 1 and 4 $M_\odot$ objects respectively. The dashed vertical line indicates the typical luminosity observed for the central stars of Planetary Nebulae (see text).

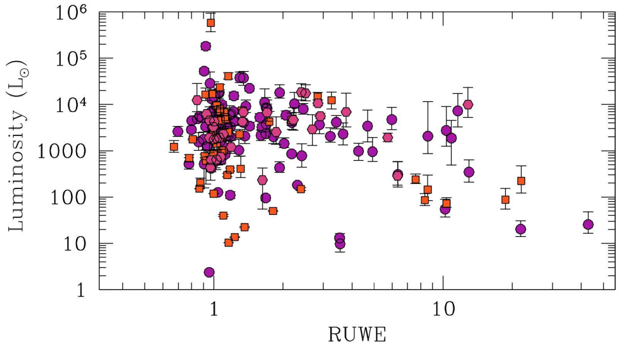

Figure 4. The luminosity as function of RUWE parameter. The plot symbols are the same as in Fig. 2.

ues are on average 1.2 ± 0.4 larger than those computed by Vickers. Although there is a systematic difference, this can be due to the uncertainty and choice of the reddening values (cf. Kamath et al. 2022). Although the literature comparison suggests that Vickers' fluxes may have been a bit underestimated, we conclude that both the uncertainties on the fluxes as well as any corrections to these are too small to explain the extent to which a large number of objects is underluminous.

Effect of parallax quality on luminosities: Next to the uncertainties on the parallax discussed above, the renormalised unit weight error (RUWE, Lindegren et al. 2021) is a powerful quality indicator of the Gaia astrometry. It measures the goodness-of-fit for the astrometric solution and is sensitive to the presence of extended emission or binary companions. It may be useful to point out that both AFGL 618 and AFGL 2688 which were mentioned earlier do not have a Gaia-based parallax measurement. These objects are very extended at optical wavelengths and determining their positions and thus parallaxes proved difficult. Fig. 4 shows the luminosity as function of RUWE. Many of the lowest luminosity stars have values far below the typical value of RUWE < 1.4 which is normally taken as of good quality. This suggests that the RUWE parameter, or the circumstances that lead to its determination, is not responsible for the large number of under-luminous objects. The objects with the highest RUWE are among the faintest, closest, objects. We suspect that more distant, more luminous objects which would otherwise receive a high RUWE value, would have their parallaxes more compromised and not be included in Gaia DR3. It appears that the parallax quality - as probed by the RUWE parameter - does not bias the results.

Vickers' classification of post-AGB nature: Vickers et al. (2015) classified objects as being a “likely” or “possible” post-AGB star and added a number of “miscellaneous” post-AGB candidates. As Figures 2 and 3 indicate, all three categories contain underluminous objects. The “likely” group - the group with the best credentials to be a post-AGB object according to Vickers et al. (2015) contains a large number of underluminous objects; 25 out of the 106 objects in the category are fainter than 1000 $L_\odot$. Almost half (22 out of 49) of the “possible” group appears to be underluminous, while 6 out of 30 “miscellaneous” stars are underluminous. It would appear that the confidence in the classification of having a post-AGB nature did not have a significant effect on whether the objects are underluminous or not.

4.1 The underluminous post-AGB stars: Galactic post-Red Giant Branch objects.

This paper presents the first census of post-AGB candidate stars in the HR diagram. Here we highlight that many objects are placed well below the widely accepted post-AGB tracks. 53 objects out of the 185 stars for which luminosities could be derived are fainter than 1000 $L_\odot$. This finding comes at the heels of Hrivnak et al. (2020) who studied 5 post-AGB stars and pointed out that 2 of these had (Gaia-DR2 based) luminosities of 1000-1500 $L_\odot$. In addition, recently, Kamath et al. (2022) reported that 4 of their 31 post-AGB stars, selected to be both “single” and being bright enough to have abundance analyses performed, were < 1000 $L_\odot$ based on their Gaia DR3 derived luminosities.

Pre-Gaia, the most reliable HR-diagram could only be constructed for extra-Galactic objects which were all at the same, known, distance. Kamath et al. (2016) found that about a third of the post-AGB candidate stars in the Magellanic Clouds were also underluminous, with values down to ∼100 $L_\odot$. These authors pointed out that Red Giant Branch (RGB) stars that have similar luminosities as the objects under consideration do not have sufficiently large mass loss rates to give rise to observable infrared excess emission. Instead, they proposed the objects are the result of binary evolution. In particular, they suggest that the stars did evolve off the RGB after a recent Common Envelope phase perhaps followed by a merger. The fraction of post-RGB candidates in their sample was in line with predictions from population synthesis models. The large number of lower luminosity stars we find appear to be the Galactic counterparts of this new class of object, confirming that these objects are numerous. Indeed, completing the evolutionary picture, post-RGB candidate stars have also been reported in Planetary Nebulae (Hillwig et al. 2017; Jones et al. 2022).

It is intriguing that although our sample is less well-defined as the Magellanic Cloud sample, we arrive at a similar fraction of post-RGB objects. We do note however that the underluminous objects are predominately found at smaller distances. A properly defined, volume-limited, sample might well increase that fraction, but this would require a well-defined sample with well-understood observational biases, which is thus far lacking for the Galaxy.

Our analysis earlier on Gaia's RUWE parameter which can be used as an indication of binarity (Belokurov et al. 2020), demonstrated that many under-luminous objects do not have large RUWE values. In that sense, they can be considered single or as an unresolved close binary (e.g. Chornay et al. 2021). Although this is very much circumstantial, the "non- or close binary" nature can be seen as consistent with the notion that they are the result of Common Envelope Evolution.

5 CONCLUDING REMARKS

We have presented the first Gaia census of post-AGB stars. From a master sample of 350 objects, we were able to determine luminosities for 185, and place 134 of these, the largest such sample ever, in the HR diagram. We find the following.

- Our principal conclusion is that although many objects are very consistent with the post-AGB evolutionary tracks, we find that 53, almost a third of this total, are underluminous and unlikely to have a post-AGB nature.
- Instead, we identify these as the Galactic counterparts of the class of post-Red Giant Branch stars recently discovered in the Magellanic Clouds. As such we report the discovery of the first sample of Galactic post-RGB stars.
- Current models suggest that these post-RGB objects are the result of binary interactions and possibly mergers. As these objects turn out to be very numerous, they will pose significant challenges to, and provide crucial new data to inform, binary star evolution and population synthesis models.

Finally, moving to the extremes, like Kamath et al. (2022) we too find objects with luninosities down to $\sim$10 $L_{\odot}$. This would be too faint to be explained by RGB progenitors which are expected to be brighter than $\sim$100 $L_{\odot}$. On the other extreme, some of the brightest, overluminous, objects ($\sim 10^{4-5}$ $L_{\odot}$), are known massive evolved stars in their post-Red Supergiant phase (Oudmaijer et al. 2009). The sample is likely to harbour more such examples. In future work we aim to study these samples in more detail.

ACKNOWLEDGMENTS

This work has made use of data from the European Space Agency (ESA) mission *Gaia* (https://www.cosmos.esa.int/gaia), processed by the *Gaia* Data Processing and Analysis Consortium (DPAC, https://www.cosmos.esa.int/web/gaia/dpac/consortium). Funding for the DPAC has been provided by national institutions, in particular the institutions participating in the *Gaia* Multilateral Agreement.

DATA AVAILABILITY

The catalogue of post-AGB stars with parallax information, their astrometric data and derived parameters used in this article are available in its online supplementary material and in Table 1.

REFERENCES

Arenou, F., Grenon, M., Gomez, A.: A&A **258**, 104 (1992)
Bailer-Jones, C.A.L., Rybizki, J., Fouesneau, M., Demleitner, M., Andrae, R.: AJ **161**(3), 147 (2021)
Belokurov, V., Penoyre, Z., Oh, S., Iorio, G., Hodgkin, S., Evans, N.W.e.a.: MNRAS **496**(2), 1922 (2020)
Bergeron, P., Saffer, R.A., Liebert, J.: ApJ **394**, 228 (1992)
Blöcker, T.: A&A **299**, 755 (1995)
Bressan, A., Marigo, P., Girardi, L., Salasnich, B., Dal Cero, C., Rubele, S., Nanni, A.: MNRAS **427**(1), 127 (2012)
Chornay, N., Walton, N.A., Jones, D., Boffin, H.M.J., Rejkuba, M., Wesson, R.: A&A **648**, 95 (2021)
Gaia Collaboration, Prusti, T., de Bruijne, J.H.J., Brown, A.G.A., Vallenari, A., Babusiaux, C., Bailer-Jones, C.A.L.e.a.: A&A **595**, 1 (2016)
Gaia Collaboration, Brown, A.G.A., Vallenari, A., Prusti, T., de Bruijne, J.H.J., Babusiaux, C., Biermann, M.e.a.: A&A **649**, 1 (2021)
González-Santamaría, I., Manteiga, M., Manchado, A., Ulla, A., Dafonte, C., López Varela, P.: A&A **656**, 51 (2021)
Herwig, F., Schönberner, D., Blöcker, T.: A&A **340**, 43 (1998)
Hillwig, T.C., Frew, D.J., Reindl, N., Rotter, H., Webb, A., Margheim, S.: AJ **153**(1), 24 (2017)
Hrivnak, B.J., Henson, G., Hillwig, T.C., Lu, W., Nault, K.A., Volk, K.: ApJ **901**(1), 9 (2020)
Jones, D., Munday, J., Corradi, R.L.M., Rodríguez-Gil, P., Boffin, H.M.J., Zak, J., Sowicka, P., Parsons, S.G., Dhillon, V.S., Littlefair, S.P., Marsh, T.R., Reindl, N., García-Rojas, J.: MNRAS **510**(2), 3102 (2022)
Kamath, D., Wood, P.R., Van Winckel, H., Nie, J.D.: A&A **586**, 5 (2016)
Kamath, D., Van Winckel, H., Ventura, P., Mohorian, M., Hrivnak, B.J., Dell'Agli, F., Karakas, A.: ApJ **927**(1), 13 (2022)
Koumpia, E., Oudmaijer, R.D., Graham, V., Banyard, G., Black, J.H., Wichittanakom, C., Ababakr, K.M., de Wit, W.-J.e.a.: A&A **635**, 183 (2020)
Lindegren, L., Klioner, S.A., Hernández, J., Bombrun, A., Ramos-Lerate, M., Steidelmüller, H.e.a.: A&A **649**, 2 (2021)
Miller Bertolami, M.M.: IAU Symposium **343**, 36 (2019)
Miller Bertolami, M.M.: A&A **588**, 25 (2016)
Ney, E.P., Merrill, K.M., Becklin, E.E., Neugebauer, G., Wynn-Williams, C.G.: ApJ **198**, 129 (1975)
Oudmaijer, R.D., Davies, B., de Wit, W.-J., Patel, M.: ASPC, vol. 412, p. 17 (2009)
Parthasarathy, M., Matsuno, T., Aoki, W.: PASJ **72**(6), 99 (2020)
Schlafly, E.F., Finkbeiner, D.P.: ApJ **737**(2), 103 (2011)
Schönberner, D.: ApJ **272**, 708 (1983)
Straizys, V., Kuriliene, G.: Ap&SS **80**(2), 353 (1981)
Suárez, O., García-Lario, P., Manchado, A., Manteiga, M., Ulla, A., Pottasch, S.R.: A&A **458**(1), 173 (2006)
Szczerba, R., Siódmiak, N., Stasińska, G., Borkowski, J.: A&A **469**(2), 799 (2007)
van Hoof, P.A.M., Oudmaijer, R.D., Waters, L.B.F.M.: MNRAS **289**(2), 371 (1997)
van Winckel, H.: ARA&A **41**, 391 (2003)
Vickers, S.B., Frew, D.J., Parker, Q.A., Bojičić, I.S.: MNRAS **447**(2), 1673 (2015)
Westbrook, W.E., Becklin, E.E., Merrill, K.M., Neugebauer, G., Schmidt, M., Willner, S.P., Wynn-Williams, C.G.: ApJ **202**, 407 (1975)

Table 1: The 249 sources from Vickers et al. (2015) for which parallax information is available. The table lists the astrometric data and the stellar parameters used in this article. Distances from Bailer-Jones et al. (2021). Last column indicates the post-AGB likelihood classification from Szczerba et al. (2007) and Vickers et al. (2015): ‘1’ for the *likely* category, ‘2’ for the *possible* category, and ‘3’ for the *miscellaneous* category.

Gaia DR3 source id	SIMBAD name	RA	DEC	SpType	$T_{\rm eff}$	Parallax	RUWE	Distance	Luminosity	Vickers
		h:m:s	deg:m:s		log([K])	[mas]		[kpc]	[$L_\odot$]	category
565507868441719424	IRAS 01005+7910	01:04:45.5	+79:26:47	B2	4.36	0.241 ± 0.018	1.037	$3.68^{+0.26}_{-0.22}$	2470^{+360}_{-290}	1
2351623413515105920	BPS CS22946-0005	01:16:52.9	-22:12:09	B	4.26	-0.036 ± 0.034	1.017	$13.8^{+3.4}_{-4.3}$	1240^{+680}_{-640}	2
4715635535640762240	LB 3193	01:18:53.3	-61:55:41			0.137 ± 0.024	0.7787	$5.71^{+0.93}_{-0.71}$	520^{+180}_{-120}	1
532078488709487360	IRAS 01259+6823	01:29:33.3	+68:39:15	F5Ie	3.81	0.62 ± 0.14	1.309	$1.78^{+0.68}_{-0.35}$	410^{+370}_{-140}	2
4686479751449676032	LB 3219	01:30:22.9	-73:03:33	B	4.26	-0.067 ± 0.024	0.9284	29^{+11}_{-9}	49000^{+45000}_{-26000}	1
351149177434709760	IRAS 01427+4633	01:45:47.0	+46:49:02	F2III	3.85	0.293 ± 0.017	1.058	$3.08^{+0.16}_{-0.13}$	1910^{+210}_{-160}	3
459182413984008448	IRAS 02143+5852	02:17:57.7	+59:05:53	F7Ie	3.79	1.36 ± 0.29	18.69	$0.85^{+0.28}_{-0.17}$	87^{+66}_{-32}	2
513671461473684352	IRAS Z02229+6208	02:26:41.6	+62:21:23	K0	3.64	0.381 ± 0.06	2.454	$2.35^{+0.34}_{-0.29}$	8000^{+2400}_{-1800}	1
433515788197481984	IRAS 02528+4350	02:56:11.3	+44:02:54	A0e	3.99	2.541 ± 0.019	1.234	$0.3899^{+0.0027}_{-0.0032}$	$13.68^{+0.19}_{-0.22}$	2
3303343395568710016	IRAS 03507+1115	03:53:28.9	+11:24:21	M7	3.47	3.84 ± 0.27	2.844	$0.260^{+0.021}_{-0.017}$	10700^{+1800}_{-1400}	3
471908436438311680	IRAS 04215+6000	04:25:50.8	+60:07:12	W9	4.643	0.153 ± 0.016	1.1	$5.23^{+0.68}_{-0.44}$	2300^{+630}_{-370}	3
173086700992466688	IRAS 04296+3429	04:32:57.0	+34:36:11	G0Ia	3.76	-0.38 ± 0.17	5.758	$5.0^{+2.1}_{-1.1}$	6200^{+6200}_{-2500}	1
255225480926107392	IRAS 05040+4820	05:07:50.4	+48:24:09	A4Ia	3.935	0.322 ± 0.014	1.02	$2.84^{+0.12}_{-0.13}$	5260^{+470}_{-460}	1
3238918336374596864	IRAS 05089+0459	05:11:36.2	+05:03:26	M3I	3.49	0.75 ± 0.35	21.91	$1.34^{+0.61}_{-0.35}$	220^{+250}_{-100}	2
3388902129107252992	IRAS 05113+1347	05:14:07.7	+13:50:29	G5I	3.7	-0.01 ± 0.15	6.663	$4.6^{+3.8}_{-1.3}$	2600^{+6000}_{-1300}	1
3422437684728294528	IRAS 05140+2851	05:17:15.5	+28:54:20	F0	3.87	0.894 ± 0.079	2.834	$1.08^{+0.12}_{-0.08}$	14600^{+3500}_{-2100}	2
2968265509022275840	IRAS 05208-2035	05:22:59.5	-20:32:52			0.687 ± 0.03	2.184	$1.403^{+0.059}_{-0.053}$	854^{+73}_{-64}	1
4758015524139610880	CPD-61 455	05:23:33.7	-60:55:28	B1	4.42	0.694 ± 0.035	1.683	$1.395^{+0.085}_{-0.077}$	95^{+12}_{-10}	1
2902505745786910080	IRAS F05338-3051	05:35:44.2	-30:49:35	G5	3.7	0.522 ± 0.016	1.094	$1.850^{+0.043}_{-0.044}$	2050^{+100}_{-100}	2
3334854780347915520	IRAS 05341+0852	05:36:55.2	+08:54:08	F6I	3.8	0.51 ± 0.19	12.96	$2.06^{+0.72}_{-0.45}$	350^{+290}_{-140}	1
3336558507975208448	IRAS 05381+1012	05:40:57.1	+10:14:25	G2I	3.73	1.038 ± 0.016	1.042	$0.937^{+0.010}_{-0.011}$	$126.4^{+2.8}_{-2.9}$	1
994259335315643520	IRAS 06338+5333	06:37:52.2	+53:31:02	F7IV:	3.79	0.268 ± 0.024	1.622	$3.40^{+0.28}_{-0.28}$	3210^{+550}_{-500}	1
3105987960396950784	IRAS 06530-0213	06:55:31.7	-02:17:27	F5Ia	3.81	0.241 ± 0.074	3.657	$3.8^{+1.2}_{-0.9}$	2300^{+1700}_{-1000}	1
3159640386918214528	IRAS 07008+1050	07:03:39.8	+10:46:12	A0	3.99	0.518 ± 0.03	1.348	$1.81^{+0.11}_{-0.11}$	4070^{+510}_{-460}	1
3108327343185135872	IRAS 07131-0147	07:15:41.8	-01:52:40	M5III	3.47	0.79 ± 0.13	8.333	$1.25^{+0.22}_{-0.16}$	86^{+32}_{-20}	2
5617989266685365120	IRAS 07140-2321	07:16:08.3	-23:27:03	F5	3.81	0.178 ± 0.012	1.029	$5.12^{+0.40}_{-0.38}$	9500^{+1600}_{-1400}	2
3156171118495247360	IRAS 07134+1005	07:16:10.3	+09:59:47	F5I	3.81	0.454 ± 0.024	0.9215	$2.10^{+0.11}_{-0.11}$	3300^{+360}_{-330}	1
3032030620730261376	IRAS 07227-1320	07:25:03.0	-13:26:20	M1I	3.56	0.489 ± 0.021	1.176	$1.982^{+0.074}_{-0.067}$	393^{+30}_{-26}	2
5620444471847839232	IRAS 07253-2001	07:27:33.0	-20:07:21	F2I	3.85	2.45 ± 0.52	42.89	$0.45^{+0.17}_{-0.09}$	$25.6^{+22.4}_{-9.2}$	1
3151417586128916864	IRAS 07430+1115	07:45:51.4	+11:08:20	M2I	3.54	3.06 ± 0.5	21.8	$0.361^{+0.082}_{-0.061}$	$20.3^{+10.2}_{-6.3}$	1
5597822402371118336	IRAS 07577-2806	07:59:46.5	-28:14:54			0.78 ± 0.16	10.21	$1.42^{+0.40}_{-0.25}$	55^{+35}_{-17}	1

Table 1 (continued).

Gaia DR3 source id	SIMBAD name	RA h:m:s	DEC deg:m:s	SpType	$T_{\rm eff}$ log([K])	Parallax [mas]	RUWE	Distance [kpc]	Luminosity [$L_\odot$]	Vickers category
5698817012142459136	IRAS 08005-2356	08:02:40.8	-24:04:44	F5Iae	3.81	-0.257 ± 0.083	5.902	$9.2^{+2.1}_{-1.7}$	54000^{+28000}_{-18000}	1
5545800762036628736	IRAS 08057-3417	08:07:40.0	-34:26:04			0.258 ± 0.025	2.062	$3.86^{+0.44}_{-0.33}$	5800^{+1400}_{-1000}	1
5520238967817034880	IRAS 08143-4406	08:16:03.1	-44:16:05	F8I	3.78	0.238 ± 0.018	1.433	$4.16^{+0.41}_{-0.28}$	3400^{+710}_{-440}	1
5707613169577769600	IRAS 08187-1905	08:20:57.2	-19:15:04	F6Ib/II	3.8	0.288 ± 0.033	1.695	$3.26^{+0.39}_{-0.34}$	3730^{+950}_{-740}	1
5540178478053582592	IRAS 08242-3828	08:26:03.7	-38:38:47			0.496 ± 0.052	1.155	$2.09^{+0.31}_{-0.23}$	2540^{+810}_{-520}	2
5277809440015969792	IRAS 08275-6206	08:28:24.5	-62:16:20			0.496 ± 0.014	1.073	$1.952^{+0.050}_{-0.057}$	629^{+32}_{-36}	1
5515266327706463616	IRAS 08281-4850	08:29:40.6	-49:00:03	F0I	3.87	-0.137 ± 0.069	6.044	$11.4^{+3.7}_{-2.7}$	8400^{+6200}_{-3500}	1
5521628033275348480	IRAS 08351-4634	08:36:45.4	-46:44:49			0.505 ± 0.05	0.9962	$1.96^{+0.19}_{-0.20}$	840^{+170}_{-160}	2
5409069172514684416	IRAS 09394-4909	09:41:14.0	-49:22:46			0.148 ± 0.041	2.407	$5.2^{+1.2}_{-0.9}$	18000^{+10000}_{-6000}	3
5462428643590805248	IRAS 10158-2844	10:18:07.5	-28:59:31	B9	4.02	0.711 ± 0.098	1.935	$1.45^{+0.31}_{-0.19}$	18000^{+8600}_{-4300}	1
5254793942926363392	IRAS 10214-6017	10:23:09.4	-60:32:43	O7	4.57	0.223 ± 0.023	1.332	$4.20^{+0.36}_{-0.37}$	4240^{+750}_{-710}	3
5351904394753372672	IRAS 10256-5628	10:27:35.3	-56:44:19	F5I	3.81	-0.09 ± 0.33	6.799	$3.8^{+2.1}_{-1.2}$	2800^{+3800}_{-1500}	1
5351069693654349952	IRAS 10456-5712	10:47:38.5	-57:28:03	M0	3.57	0.9 ± 0.026	0.984	$1.104^{+0.035}_{-0.029}$	16800^{+1100}_{-900}	2
5241806275407841664	IRAS 11000-6153	11:02:04.4	-62:09:44	F2III	3.85	0.221 ± 0.015	1.062	$4.40^{+0.29}_{-0.29}$	23700^{+3200}_{-3100}	2
5337582534294739456	IRAS 11159-5954	11:18:07.3	-60:10:39			-0.29 ± 0.13	2.095	$7.0^{+2.3}_{-1.5}$	4500^{+3500}_{-1700}	2
5237007177683569536	IRAS 11201-6545	11:22:18.8	-66:01:49	A3Ie	3.95	0.24 ± 0.13	10.32	$4.5^{+3.6}_{-1.5}$	2700^{+6200}_{-1500}	1
5335866849446446080	IRAS 11339-6004	11:36:20.9	-60:20:53			0.08 ± 0.3	1.026	$4.7^{+2.8}_{-2.0}$	800^{+1200}_{-500}	1
5335709477519159936	IRAS 11353-6037	11:37:43.1	-60:53:50	B5Ie	4.18	0.169 ± 0.013	1.101	$5.42^{+0.38}_{-0.38}$	2550^{+370}_{-340}	1
5332682659443937664	IRAS 11381-6401	11:40:31.7	-64:18:26			-0.09 ± 0.2	0.9462	$6.0^{+2.6}_{-1.7}$	4700^{+4900}_{-2200}	1
5343168568718268800	IRAS 11385-5517	11:40:58.9	-55:34:27	B8	4.06	0.545 ± 0.02	1.054	$1.788^{+0.057}_{-0.066}$	17400^{+1200}_{-1200}	1
5335675087769798272	IRAS 11387-6113	11:41:08.7	-61:30:19	A3Ie	3.95	0.185 ± 0.018	1.179	$5.02^{+0.64}_{-0.47}$	3250^{+880}_{-580}	1
3589047952995134720	IRAS 11472-0800	11:49:48.0	-08:17:21			0.11 ± 0.084	4.678	$6.1^{+3.0}_{-2.0}$	3400^{+4200}_{-1800}	1
3492184311482349824	EC 11507-2253	11:53:15.9	-23:09:53	B5	4.18	-0.001 ± 0.038	0.9783	$11.0^{+4.8}_{-2.4}$	330^{+350}_{-130}	1
5335102207846402176	IRAS 11531-6111	11:55:37.8	-61:28:16	B8Ie	4.06	0.158 ± 0.018	0.9739	$5.27^{+0.46}_{-0.43}$	416^{+75}_{-65}	1
5332853912685160064	IRAS 11544-6408	11:56:57.2	-64:25:16			-0.55 ± 0.84	1.23	$4.6^{+2.5}_{-1.5}$	4200^{+5900}_{-2300}	1
3920735495441657728	BD+13 2491	12:07:10.9	+12:59:07	B9	4.02	0.597 ± 0.027	0.798	$1.567^{+0.065}_{-0.064}$	2860^{+240}_{-230}	1
6076326701687231872	IRAS 12175-5338	12:20:15.0	-53:55:29	A7I	3.9	-0.009 ± 0.066	3.651	$8.7^{+3.8}_{-2.2}$	20000^{+21000}_{-9000}	1
3469106382752903168	CD-31 9638	12:20:45.0	-32:33:25	A2II/III	3.96	0.367 ± 0.021	1.12	$2.57^{+0.14}_{-0.14}$	831^{+91}_{-88}	1
6130448958959242240	IRAS 12222-4652	12:24:53.4	-47:09:09	F4	3.82	0.17 ± 0.03	1.298	$5.13^{+0.79}_{-0.60}$	38000^{+13000}_{-8000}	1
6053621271182676352	IRAS 12302-6317	12:33:07.5	-63:33:41			-0.57 ± 0.14	1.307	$11.1^{+5.1}_{-3.3}$	13000^{+15000}_{-7000}	1
6058372329633216896	IRAS 12309-5928	12:33:44.5	-59:45:18			-3.6 ± 1.8	2.33	$5.3^{+2.9}_{-1.9}$	1000^{+1400}_{-600}	1

Table 1 (continued).

Gaia DR3 source id	SIMBAD name	RA h:m:s	DEC deg:m:s	SpType	$T_{\rm eff}$ log([K])	Parallax [mas]	RUWE	Distance [kpc]	Luminosity [$L_\odot$]	Vickers category
6060828565581083264	IRAS 12360-5740	12:38:53.2	-57:56:31	F0	3.87	0.091 ± 0.014	1.07	$9.1^{+1.1}_{-0.8}$	4500^{+1200}_{-800}	2
6073662099660289536	IRAS 12419-5414	12:44:46.1	-54:31:12			2.69 ± 0.13	3.534	$0.365^{+0.017}_{-0.017}$	$13.1^{+1.3}_{-1.2}$	1
3497154104039422848	IRAS 12538-2611	12:56:30.1	-26:27:36	F3Ia	3.83	0.567 ± 0.023	0.9709	$1.684^{+0.085}_{-0.065}$	6750^{+690}_{-510}	1
6084869868362934144	IRAS 12584-4837	13:01:17.6	-48:53:20	B5e	4.18	1.59 ± 0.15	7.593	$0.649^{+0.093}_{-0.063}$	241^{+74}_{-45}	2
6055883241501706752	IRAS 13010-6012	13:04:05.3	-60:28:46			-0.02 ± 0.18	7.212	$5.5^{+2.5}_{-1.6}$	550^{+620}_{-280}	2
5863599857739835264	IRAS 13064-6103	13:09:36.3	-61:19:37	B	4.26	-1.36 ± 0.37	25.79	$4.5^{+1.8}_{-1.3}$	16000^{+15000}_{-8000}	3
6066902993687172608	IRAS 13110-5425	13:14:08.4	-54:41:34	F5Ia/ab	3.81	0.64 ± 0.031	1.06	$1.535^{+0.071}_{-0.067}$	2510^{+240}_{-210}	1
5857811238294426752	IRAS 13110-6629	13:14:26.8	-66:45:33			0.235 ± 0.021	0.8677	$4.00^{+0.30}_{-0.30}$	5550^{+860}_{-800}	1
5869845594859880064	IRAS 13203-5917	13:23:32.2	-59:32:50	G2I	3.73	0.183 ± 0.042	3.218	$5.4^{+1.2}_{-0.7}$	2100^{+1100}_{-500}	1
3624198034063995008	BPS CS22877-0023	13:25:39.5	-08:49:21	B3	4.26	0.056 ± 0.028	1.076	$9.6^{+4.4}_{-1.8}$	820^{+940}_{-280}	1
6083719439934104832	CD-46 8644	13:26:26.2	-47:16:27	A7	3.9	0.177 ± 0.02	0.933	$4.89^{+0.44}_{-0.38}$	1240^{+240}_{-180}	1
6083708479176016128	Cl* NGC 5139WOR1957	13:27:28.9	-47:22:48			0.115 ± 0.03	0.9013	$6.2^{+1.3}_{-0.8}$	1760^{+780}_{-420}	1
6070128028770373888	IRAS 13245-5036	13:27:37.1	-50:52:05	A7	3.9	0.012 ± 0.022	1.605	$14.2^{+3.2}_{-2.9}$	6900^{+3400}_{-2500}	1
6063703586653222144	IRAS 13266-5551	13:29:51.1	-56:06:53	B1Iae	4.42	0.338 ± 0.02	1.141	$2.82^{+0.16}_{-0.14}$	3560^{+420}_{-360}	1
5783415017323438848	IRAS 13258-8103	13:31:06.3	-81:18:30	F8	3.78	0.72 ± 0.21	8.569	$1.61^{+0.70}_{-0.38}$	140^{+150}_{-60}	2
5870113880062711552	IRAS 13313-5838	13:34:37.4	-58:53:33	K5I	3.59	1.09 ± 0.13	10.35	$0.96^{+0.15}_{-0.09}$	72^{+24}_{-13}	2
5865398796206273152	IRAS 13356-6249	13:39:06.4	-63:04:45			0.284 ± 0.093	1.171	$2.99^{+0.81}_{-0.64}$	5900^{+3600}_{-2200}	1
5869018899564351872	IRAS 13398-5951	13:43:12.4	-60:07:04			1.53 ± 0.59	1.628	$2.3^{+0.8}_{-1.2}$	230^{+190}_{-180}	3
5864661779824561664	IRAS 13416-6243	13:45:07.2	-62:58:15	G1I	3.745	0.21 ± 0.1	1.002	$4.4^{+2.0}_{-1.1}$	15000^{+16000}_{-6000}	1
5867561191994328704	IRAS 13529-5934	13:56:24.9	-59:48:58			-0.91 ± 0.98	2.641	$3.9^{+1.6}_{-1.7}$	760^{+760}_{-510}	1
5896479309853592448	IRAS 14072-5446	14:10:39.0	-55:00:27	A3I	3.95	0.207 ± 0.014	0.8488	$4.34^{+0.26}_{-0.24}$	4860^{+600}_{-520}	1
5853777267581362176	IRAS 14103-6311	14:14:09.3	-63:25:47	M0	3.57	0.28 ± 0.18	12.84	$3.8^{+2.0}_{-1.0}$	10000^{+13000}_{-5000}	3
5849962851220246016	IRAS 14325-6428	14:36:34.5	-64:41:31	F5I	3.81	0.192 ± 0.037	2.181	$4.88^{+0.93}_{-0.62}$	4600^{+1900}_{-1100}	2
5849958457496943744	IRAS 14331-6435	14:37:10.3	-64:48:06	B3Ie	4.26	0.351 ± 0.058	3.417	$2.91^{+0.53}_{-0.44}$	4100^{+1600}_{-1100}	1
5877302177877393024	IRAS 14341-6211	14:38:05.1	-62:24:49			-0.12 ± 0.18	1.815	$7.8^{+4.2}_{-2.7}$	3500^{+4900}_{-2000}	1
5878583349370477312	IRAS 14346-5952	14:38:24.6	-60:04:52			0.261 ± 0.096	1.126	$3.1^{+1.0}_{-0.7}$	4900^{+3500}_{-2000}	2
5906408788891928704	IRAS 14429-4539	14:46:13.7	-45:52:07	G0Ie	3.76	-0.11 ± 0.51	2.788	$3.8^{+2.7}_{-1.7}$	3100^{+5800}_{-2100}	1
5880708980232408448	IRAS 14482-5725	14:51:58.2	-57:38:17	A2I	3.96	0.358 ± 0.049	1.935	$2.50^{+0.39}_{-0.28}$	430^{+140}_{-90}	1
5893945588395282304	IRAS 14488-5405	14:52:28.9	-54:17:43	A0Ie	3.99	0.268 ± 0.017	1.327	$3.42^{+0.21}_{-0.19}$	7400^{+1000}_{-800}	2
5899715786733345536	IRAS 14562-5406	14:59:53.5	-54:18:09	W9.	4.643	0.482 ± 0.027	1.346	$1.94^{+0.10}_{-0.08}$	6830^{+700}_{-540}	3
5903310335089068416	IRAS 15039-4806	15:07:27.2	-48:17:53	A5Iab	3.92	0.563 ± 0.026	0.8877	$1.708^{+0.074}_{-0.061}$	5200^{+460}_{-360}	1

Table 1 (continued).

Gaia DR3 source id	SIMBAD name	RA h:m:s	DEC deg:m:s	SpType	$T_{\rm eff}$ log([K])	Parallax [mas]	RUWE	Distance [kpc]	Luminosity [$L_\odot$]	Vickers category
5886573569080505216	IRAS 15066-5532	15:10:26.6	-55:44:13			0.261 ± 0.025	1.181	$3.23^{+0.24}_{-0.20}$	2010^{+310}_{-240}	1
5877154701494366336	IRAS 15103-5754	15:14:18.7	-58:05:20			0.31 ± 0.81	1.092	$3.7^{+1.9}_{-1.7}$	7200^{+9300}_{-5200}	3
5877096736611221888	IRAS 15144-5812	15:18:21.9	-58:23:13			-0.018 ± 0.08	1.06	$7.3^{+2.1}_{-1.9}$	16000^{+10000}_{-7000}	2
5888049732191403904	IRAS 15154-5258	15:19:08.7	-53:09:51	W4	5.068	0.299 ± 0.024	1.027	$2.89^{+0.20}_{-0.21}$	644^{+93}_{-90}	3
5824126771840487936	IRAS 15210-6554	15:25:31.5	-66:05:20	K2I	3.62	-0.15 ± 0.14	2.279	$7.5^{+2.6}_{-2.8}$	4600^{+3700}_{-2800}	1
1194929381434604800	IRAS F15240+1452	15:26:20.9	+14:41:36	B9Iab:p	4.02	0.752 ± 0.079	2.023	$1.32^{+0.20}_{-0.13}$	1440^{+460}_{-270}	1
1369896865785991424	BD+33 2642	15:51:59.8	+32:56:54	O7p	4.57	0.271 ± 0.032	1.295	$3.47^{+0.47}_{-0.31}$	2260^{+650}_{-380}	2
5996617434442714880	IRAS 16029-4101	16:06:24.4	-41:09:57			0.2 ± 0.069	4.272	$4.3^{+1.0}_{-0.9}$	980^{+480}_{-360}	1
5933063252888145920	IRAS 16086-5255	16:12:30.6	-53:03:11			0.358 ± 0.014	0.912	$2.50^{+0.12}_{-0.10}$	771^{+79}_{-58}	2
5835411094089870592	IRAS 16099-5651	16:14:01.4	-56:59:28	M8	3.47	0.34 ± 0.11	0.8452	$3.9^{+2.0}_{-1.0}$	12000^{+16000}_{-5000}	3
5935061172876722176	IRAS 16115-5044	16:15:17.9	-50:52:21			0.291 ± 0.09	0.9794	$3.05^{+0.80}_{-0.80}$	13100^{+7900}_{-6000}	1
5990014935825542144	IRAS 16130-4620	16:16:42.9	-46:27:53			-0.89 ± 0.54	1.115	$5.4^{+3.5}_{-1.9}$	2900^{+5000}_{-1700}	2
5934701559547878144	IRAS 16133-5151	16:17:13.2	-51:59:11	B0	4.49	0.366 ± 0.086	2.51	$2.65^{+0.62}_{-0.46}$	17400^{+9100}_{-5500}	3
5932016212933920384	LS 3593	16:24:39.4	-54:38:08	A0Ib	3.99	0.443 ± 0.019	0.8017	$2.138^{+0.091}_{-0.080}$	4450^{+390}_{-330}	1
5831295999979910656	IRAS 16206-5956	16:25:02.9	-60:03:32	A0Iae	3.99	0.182 ± 0.019	1.066	$5.02^{+0.66}_{-0.41}$	6000^{+1700}_{-1000}	1
4351018375858237952	IRAS F16277-0724	16:30:30.1	-07:30:52	A7Ib	3.9	0.281 ± 0.025	1.156	$3.10^{+0.29}_{-0.21}$	40700^{+7900}_{-5200}	2
5941189713256986752	IRAS 16279-4757	16:31:38.8	-48:04:07	M3II	3.49	-0.08 ± 0.19	1.465	$4.5^{+2.0}_{-1.3}$	28000^{+31000}_{-14000}	1
5943899425344608000	IRAS 16283-4424	16:31:57.6	-44:31:25			-0.095 ± 0.039	2.773	$13.8^{+3.2}_{-2.9}$	11100^{+5700}_{-4100}	1
1324742534573959424	BD+32 2754	16:36:11.9	+32:29:21	F8	3.78	3.239 ± 0.014	1.161	$0.3067^{+0.0012}_{-0.0012}$	$10.340^{+0.090}_{-0.080}$	2
5943047784868946688	IRAS 16328-4517	16:36:25.8	-45:24:04			0.64 ± 0.2	6.352	$1.94^{+0.73}_{-0.52}$	310^{+280}_{-140}	1
5941041038676090112	IRAS 16333-4807	16:37:06.8	-48:13:43			0.364 ± 0.024	1.003	$2.43^{+0.14}_{-0.11}$	1750^{+210}_{-160}	3
1328057763997734144	Cl* NGC 6205BARN29	16:41:33.8	+36:26:11	B2p	4.36	0.077 ± 0.03	1.157	$9.0^{+2.7}_{-1.9}$	2200^{+1500}_{-800}	1
4334241408966611328	IRAS 16476-1122	16:50:24.3	-11:27:58	M1I	3.56	0.471 ± 0.031	1.099	$1.98^{+0.13}_{-0.12}$	1010^{+140}_{-120}	2
5969973999973524224	IRAS 16494-3930	16:52:55.4	-39:34:58			0.33 ± 0.059	1.014	$2.92^{+0.56}_{-0.41}$	590^{+250}_{-150}	1
4365451214021224320	LS IV-04_1	16:56:27.8	-04:47:24	B	4.26	0.033 ± 0.017	1.03	$10.9^{+1.5}_{-1.4}$	4200^{+1300}_{-1000}	1
6029425384023553792	IRAS 16559-2957	16:59:08.2	-30:01:41	F5I(e)	3.81	-2.03 ± 0.5	23.13	$7.2^{+2.7}_{-1.9}$	10400^{+9100}_{-4700}	1
5963059480546004608	IRAS 16594-4656	17:03:10.0	-47:00:29	B7	4.1	0.546 ± 0.073	0.6971	$1.72^{+0.24}_{-0.19}$	2600^{+760}_{-550}	1
5965575811694758784	IRAS 17009-4154	17:04:29.8	-41:58:38			-2.73 ± 0.86	1.26	$6.0^{+4.5}_{-2.8}$	18000^{+37000}_{-13000}	1
4568163710366782848	PG 1704+222	17:06:46.2	+22:05:51	B3	4.26	0.091 ± 0.025	0.9389	$7.5^{+1.8}_{-1.2}$	1240^{+690}_{-370}	1
5917195002285834240	IRAS 17047-5650	17:09:00.8	-56:54:48	W9	4.643	0.678 ± 0.047	2.916	$1.48^{+0.11}_{-0.10}$	5580^{+850}_{-700}	3
5973374200987325056	IRAS 17067-3759	17:10:08.3	-38:03:23			-0.1 ± 0.31	0.9856	$4.5^{+2.2}_{-1.6}$	1100^{+1300}_{-600}	2

Table 1 (continued).

Gaia DR3 source id	SIMBAD name	RA h:m:s	DEC deg:m:s	SpType	T$_{\rm eff}$ log([K])	Parallax [mas]	RUWE	Distance [kpc]	Luminosity [L$_\odot$]	Vickers category
4128590918794710272	IRAS 17074-1845	17:10:24.0	-18:49:01	B5Ibe	4.18	0.072 ± 0.042	1.707	$8.0^{+1.9}_{-1.6}$	8200^{+4200}_{-2900}	1
4128590918794710272	IRAS 17074-1845	17:10:24.0	-18:49:01	B5Ibe	4.18	0.072 ± 0.042	1.707	$8.0^{+1.9}_{-1.6}$	6700^{+3500}_{-2400}	3
5980714063986945920	IRAS 17106-3046	17:13:51.8	-30:49:42	F5I	3.81	-0.06 ± 0.16	4.161	$7.2^{+2.3}_{-2.0}$	12800^{+9400}_{-6200}	1
5971985036767008256	IRAS 17130-4029	17:16:28.9	-40:32:30			-0.24 ± 0.48	1.961	$5.6^{+2.9}_{-2.1}$	1200^{+1500}_{-700}	2
5972460442434579968	IRAS 17163-3907	17:19:49.3	-39:10:37			0.126 ± 0.065	0.9698	$5.2^{+1.4}_{-1.0}$	$580000^{+350000}_{-210000}$	2
4058987022459300096	IRAS 17183-3017	17:21:31.9	-30:20:50			0.01 ± 0.23	3.618	$7.2^{+2.2}_{-2.1}$	6700^{+4600}_{-3300}	3
4108072721831278976	IRAS 17195-2710	17:22:43.6	-27:13:38			0.12 ± 0.4	2.942	$6.9^{+2.5}_{-2.8}$	8100^{+7000}_{-5300}	1
4136944866387751552	IRAS 17203-1534	17:23:11.9	-15:37:16	B1IIIpe	4.42	0.066 ± 0.025	1.379	$7.9^{+1.3}_{-1.2}$	9200^{+3300}_{-2500}	1
4109870908774509184	IRAS 17209-2556A	17:24:01.4	-25:59:23	W9	4.643	0.17 ± 0.032	1.189	$5.10^{+0.93}_{-0.71}$	1200^{+480}_{-310}	3
5972489407656030720	IRAS 17208-3859	17:24:19.5	-39:01:48	A2I	3.96	0.68 ± 0.49	0.9974	$5.0^{+2.7}_{-2.6}$	3200^{+4300}_{-2400}	1
4109553493474085504	IRAS 17223-2659	17:25:26.5	-27:02:01			0.163 ± 0.057	1.747	$5.2^{+1.5}_{-1.2}$	4200^{+2800}_{-1700}	2
5960186761599871488	IRAS 17234-4008	17:26:56.1	-40:11:02			0.2 ± 0.1	1.063	$5.4^{+3.5}_{-1.5}$	1600^{+2700}_{-800}	1
5975007147549090432	IRAS 17251-3505	17:28:27.7	-35:07:33			0.59 ± 0.23	0.9569	$2.4^{+1.1}_{-0.8}$	1900^{+2200}_{-1000}	3
4162959693758887424	IRAS 17279-1119	17:30:46.8	-11:22:10	F2/3II	3.85	0.201 ± 0.016	1.022	$4.27^{+0.31}_{-0.29}$	9300^{+1400}_{-1200}	1
5975083327400970752	IRAS 17277-3506	17:31:04.1	-35:08:41	B4	4.22	0.743 ± 0.025	1.111	$1.285^{+0.051}_{-0.042}$	6800^{+550}_{-440}	2
4110550475656804864	IRAS 17291-2402	17:32:12.8	-24:04:59			0.74 ± 0.4	10.87	$3.8^{+2.1}_{-1.8}$	1900^{+2600}_{-1400}	1
4061265519768800768	IRAS 17317-2743	17:34:53.6	-27:45:13	F5I	3.81	-0.06 ± 0.12	2.93	$8.3^{+2.4}_{-2.2}$	8700^{+5700}_{-4000}	1
5946845601071213696	IRAS 17311-4924	17:35:02.4	-49:26:27	B1Iae	4.42	0.238 ± 0.02	1.084	$3.86^{+0.29}_{-0.21}$	10000^{+1500}_{-1100}	1
4117592465329067008	IRAS 17332-2215	17:36:17.0	-22:17:20	K2I	3.62	3.2 ± 0.57	3.549	$0.35^{+0.10}_{-0.06}$	$9.7^{+6.6}_{-3.2}$	1
5955201232284272384	[DSH2001] 279-19	17:39:02.3	-45:00:38			0.174 ± 0.022	0.8732	$4.71^{+0.58}_{-0.41}$	204^{+53}_{-34}	2
4060159376692627840	IRAS 17358-2854	17:39:02.9	-28:56:37			0.381 ± 0.034	0.9727	$2.28^{+0.15}_{-0.16}$	626^{+84}_{-86}	3
4117263131638476032	IRAS 17360-2142	17:39:05.8	-21:43:52			-0.21 ± 0.19	4.72	$7.2^{+1.8}_{-2.0}$	3500^{+2000}_{-1700}	1
4053492968991830400	IRAS 17370-3357	17:40:20.1	-33:59:15			0.47 ± 0.68	1.098	$8.1^{+2.8}_{-3.4}$	4300^{+3600}_{-2900}	1
4118178784208141568	IRAS 17376-2040	17:40:38.7	-20:41:52			-3.3 ± 1.1	1.036	$7.0^{+2.2}_{-1.9}$	6800^{+4800}_{-3100}	2
4124125282361429504	IRAS 17381-1616	17:41:00.1	-16:18:13	B1Ibe	4.42	0.109 ± 0.025	1.148	$6.4^{+1.1}_{-0.8}$	3000^{+1100}_{-700}	1
4053880649927702656	IRAS 17385-3332	17:41:52.4	-33:33:41			-0.25 ± 0.16	3.945	$9.1^{+3.2}_{-2.9}$	5400^{+4500}_{-2900}	1
1367102319545324288	IRAS 17436+5003	17:44:55.3	+50:02:39	F3Ib	3.83	0.502 ± 0.024	1.216	$1.92^{+0.10}_{-0.09}$	6980^{+700}_{-650}	1
4120637086125583360	IRAS 17423-1755	17:45:14.1	-17:56:47	B7e	4.1	0.31 ± 0.3	1.665	$5.3^{+2.2}_{-1.4}$	11000^{+11000}_{-5000}	1
4120632688077368192	IRAS 17433-1750	17:46:15.7	-17:51:47			0.032 ± 0.02	0.9203	$9.6^{+1.7}_{-1.3}$	16400^{+6200}_{-4200}	2
4041945343757244160	IRAS 17440-3310	17:47:22.6	-33:11:08	F3I	3.83	-0.16 ± 0.12	0.7693	$8.3^{+2.4}_{-2.0}$	8000^{+5200}_{-3400}	1
5954670408684703872	IRAS 17476-4446	17:51:16.5	-44:47:30	B7Ie	4.1	0.128 ± 0.027	1.285	$6.2^{+1.9}_{-0.9}$	1030^{+730}_{-270}	1

Table 1 (continued).

Gaia DR3 source id	SIMBAD name	RA h:m:s	DEC deg:m:s	SpType	$T_{\rm eff}$ log([K])	Parallax [mas]	RUWE	Distance [kpc]	Luminosity [$L_\odot$]	Vickers category
4056355822397882880	IRAS 17480-3023	17:51:19.0	-30:23:52	W9	4.643	0.083 ± 0.062	0.9587	$8.2^{+3.3}_{-2.0}$	4500^{+4400}_{-2000}	3
4119492494479957760	IRAS 17487-1922	17:51:45.0	-19:23:45			-0.84 ± 0.49	3.084	$5.9^{+3.1}_{-2.2}$	3500^{+4600}_{-2100}	1
4067343654354938112	IRAS 17516-2525	17:54:43.3	-25:26:29	B0	4.49	0.19 ± 0.073	0.9617	$4.3^{+1.4}_{-1.2}$	28000^{+22000}_{-13000}	1
4582795323914832000	IRAS 17534+2603	17:55:25.1	+26:03:00	F2Ibp	3.85	0.761 ± 0.061	1.223	$1.31^{+0.13}_{-0.11}$	15300^{+3200}_{-2400}	1
4172337943816530432	IRAS 17542-0603	17:56:56.0	-06:04:10			0.1 ± 0.086	5.976	$5.9^{+2.1}_{-1.3}$	4700^{+3900}_{-1900}	1
4035783611879028736	IRAS 17567-3849	17:57:47.7	-38:34:12			-0.21 ± 0.21	3.581	$7.2^{+3.4}_{-2.2}$	6900^{+8200}_{-3500}	3
4062759511236966016	IRAS 17550-2800	17:58:10.4	-28:00:31			-0.08 ± 0.21	1.578	$7.1^{+3.5}_{-2.1}$	3500^{+4300}_{-1800}	2
4062301564840251520	IRAS 17574-2921	18:00:37.6	-29:21:50	W9	4.643	0.091 ± 0.052	1.03	$7.7^{+2.1}_{-1.9}$	1800^{+1200}_{-800}	3
4062817927079802240	IRAS 18022-2822	18:05:25.7	-28:22:03	W9	4.643	0.237 ± 0.043	1.073	$3.92^{+0.82}_{-0.66}$	740^{+340}_{-230}	3
4042544062195042176	IRAS 18023-3409	18:05:38.4	-34:09:31	B9Ia+e	4.02	0.022 ± 0.027	1.138	$9.4^{+1.1}_{-1.2}$	23200^{+6000}_{-5700}	1
4035907203854415488	IRAS 18025-3906	18:06:03.3	-39:05:56	G2I	3.73	0.54 ± 0.19	8.582	$3.0^{+4.1}_{-1.1}$	2100^{+9400}_{-1200}	1
4579182637944779264	IRAS 18062+2410	18:08:19.9	+24:10:44	B1IIIe	4.42	0.143 ± 0.049	2.886	$4.5^{+1.1}_{-0.9}$	3600^{+2000}_{-1300}	1
4065774307705264384	IRAS 18061-2505	18:09:12.4	-25:04:33	W8	4.778	0.55 ± 0.12	0.9664	$2.18^{+0.71}_{-0.60}$	430^{+330}_{-200}	3
4158154754919296000	IRAS 18075-0924	18:10:15.1	-09:23:34	G2I	3.73	-0.17 ± 0.19	7.58	$6.9^{+2.8}_{-2.5}$	9700^{+9200}_{-5700}	1
4093773847992815744	IRAS 18083-2155	18:11:19.8	-21:54:59			-0.51 ± 0.4	0.9837	$6.7^{+3.7}_{-2.7}$	7000^{+10000}_{-5000}	1
4580154606223711872	IRAS 18095+2704	18:11:30.5	+27:05:15	F3Ib	3.83	0.03 ± 0.18	13.74	$4.9^{+1.7}_{-1.6}$	17000^{+13000}_{-9000}	1
4049331244394134912	IRAS 18129-3053	18:13:58.6	-30:36:57	W9	4.643	0.34 ± 0.11	3.771	$4.0^{+2.3}_{-1.2}$	7000^{+11000}_{-4000}	3
4065347387968755328	IRAS 18113-2503	18:14:27.2	-25:03:01			0.144 ± 0.035	1.123	$5.2^{+1.0}_{-0.8}$	2010^{+810}_{-550}	1
4049379725984965120	LS 4825	18:16:00.5	-30:45:24	B1Ib	4.42	0.003 ± 0.018	0.4916	$10.0^{+1.3}_{-0.8}$	9500^{+2800}_{-1500}	2
4065322923848085760	IRAS 18170-2416	18:20:08.8	-24:15:04	W9	4.643	0.033 ± 0.032	0.9947	$8.6^{+2.1}_{-1.2}$	3300^{+1800}_{-900}	3
4046476534251259904	CD-30 15602	18:22:42.6	-30:14:40	G0:	3.76	0.118 ± 0.025	0.6698	$5.59^{+0.93}_{-0.71}$	1220^{+440}_{-290}	2
4270080782317422208	IRAS 18240-0244	18:26:40.2	-02:42:57	W7	4.851	0.15 ± 0.22	0.7685	$4.1^{+1.5}_{-1.7}$	5000^{+4300}_{-3300}	3
4155847571502019840	IRAS 18286-0959	18:31:22.9	-09:57:20			0.5 ± 0.58	1.027	$3.3^{+2.6}_{-1.4}$	7000^{+15000}_{-5000}	1
4093689116883710592	IRAS 18313-1738	18:34:16.2	-17:36:15	B	4.26	1.244 ± 0.051	2.397	$0.793^{+0.033}_{-0.030}$	148^{+13}_{-11}	2
4104509518289438720	IRAS 18321-1401	18:34:57.6	-13:58:49			2.7 ± 1.3	0.9067	$5.5^{+3.1}_{-2.5}$	520^{+740}_{-360}	1
2096072103492979584	V534 Lyr	18:37:58.9	+37:26:06	A0Iabe	3.99	0.538 ± 0.025	1.081	$1.807^{+0.084}_{-0.081}$	1930^{+180}_{-170}	2
6736747708089687936	IRAS 18371-3159	18:40:21.9	-31:56:49	B1Iabe	4.42	0.085 ± 0.024	0.9848	$7.3^{+1.3}_{-0.9}$	3200^{+1300}_{-700}	1
4099619470274753408	IRAS 18379-1707	18:40:48.7	-17:04:39	B1IIIep	4.42	0.142 ± 0.023	0.9967	$5.35^{+0.69}_{-0.55}$	3270^{+900}_{-640}	1
4508727788268978176	IRAS 18385+1350	18:40:51.8	+13:52:51			0.029 ± 0.08	0.9762	$7.4^{+2.5}_{-1.9}$	1040^{+840}_{-470}	1
4072427555640528000	IRAS 18384-2800	18:41:37.0	-27:57:01	F2/3Ia	3.85	0.11 ± 0.027	1.346	$7.0^{+1.3}_{-1.2}$	37000^{+15000}_{-12000}	1
4253622708258596736	IRAS 18420-0512	18:44:41.7	-05:09:15			-0.33 ± 0.21	1.105	$7.6^{+2.6}_{-2.1}$	7200^{+6000}_{-3500}	2

Table 1 (continued).

Gaia DR3 source id	SIMBAD name	RA h:m:s	DEC deg:m:s	SpType	$T_{\rm eff}$ log([K])	Parallax [mas]	RUWE	Distance [kpc]	Luminosity [$L_\odot$]	Vickers category
4266422531037747200	IRAS 18454+0001	18:48:01.2	+00:04:50			0.63 ± 0.71	1.204	$4.6^{+2.4}_{-2.2}$	1200^{+1600}_{-900}	2
4285847607265349632	IRAS 18485+0642	18:50:59.7	+06:46:00			0.5 ± 0.51	1.706	$3.5^{+1.7}_{-1.5}$	1400^{+1700}_{-1000}	1
4252449701157768960	IRAS 18489-0629	18:51:39.2	-06:26:06			-0.018 ± 0.056	2.337	$10.1^{+2.7}_{-1.9}$	41000^{+24000}_{-14000}	1
4203848980711226112	Cl* NGC6712SSC26	18:53:05.7	-08:42:36			0.089 ± 0.016	0.7811	$7.63^{+0.62}_{-0.71}$	700^{+120}_{-120}	2
4282499452616310912	IRAS 18539+0549	18:56:22.7	+05:53:00			0.906 ± 0.023	1.1	$1.083^{+0.031}_{-0.027}$	$39.8^{+2.3}_{-1.9}$	2
4265817151122002688	IRAS 18582+0001	19:00:49.0	+00:06:14			0.0 ± 0.47	1.057	$5.8^{+3.2}_{-2.4}$	5100^{+7200}_{-3400}	1
4080575933190651008	IRAS 19016-2330	19:04:43.5	-23:26:10			1.08 ± 0.28	6.334	$1.02^{+0.43}_{-0.21}$	290^{+290}_{-110}	3
6715619076008049792	LSE 148	19:07:07.9	-41:43:18	B5	4.18	0.859 ± 0.049	1.093	$1.130^{+0.060}_{-0.053}$	1250^{+140}_{-120}	1
4293369057089082112	IRAS 19075+0432	19:09:59.8	+04:37:09			0.161 ± 0.027	1.119	$4.90^{+0.79}_{-0.60}$	5300^{+1800}_{-1200}	2
4264026012336768000	IRAS 19114+0002	19:13:58.7	+00:07:32	G2Ia	3.73	0.189 ± 0.021	0.9219	$4.43^{+0.35}_{-0.35}$	181000^{+30000}_{-28000}	1
4520072476226779520	IRAS 19134+2131	19:15:35.1	+21:36:34			0.13 ± 0.82	1.601	$5.8^{+2.9}_{-2.5}$	2800^{+3500}_{-1900}	1
6435349718091211264	LSE 237	19:18:49.1	-64:35:32	B5	4.18	0.069 ± 0.038	0.8585	$7.7^{+2.0}_{-1.5}$	1550^{+910}_{-540}	1
4515084168071571840	IRAS 19181+1806	19:20:24.8	+18:11:43			0.47 ± 0.56	2.219	$5.2^{+2.9}_{-3.0}$	700^{+1000}_{-600}	2
2049984454412871296	IRAS 19200+3457	19:21:55.3	+35:02:57	B8	4.06	0.025 ± 0.019	1.066	$10.3^{+2.0}_{-1.3}$	7200^{+3100}_{-1700}	2
4516723883521069952	IRAS 19207+2023	19:22:55.9	+20:28:55	F6I	3.8	-0.41 ± 0.13	8.057	$9.9^{+3.8}_{-2.7}$	5700^{+5200}_{-2700}	1
2018131400704379648	IRAS 19255+2123	19:27:43.9	+21:30:04			0.17 ± 0.11	1.004	$4.9^{+2.3}_{-1.5}$	4300^{+4900}_{-2300}	3
6744366945682210560	IRAS 19288-3419	19:32:06.8	-34:12:59	W4	5.068	-0.52 ± 0.46	13.91	$5.8^{+3.9}_{-2.0}$	190^{+360}_{-110}	3
4318134628803970816	IRAS 19306+1407	19:32:54.9	+14:13:36	B0-1I	4.49	0.085 ± 0.059	1.688	$7.1^{+2.1}_{-1.7}$	8500^{+5600}_{-3600}	1
2025220089635846528	IRAS 19309+2646	19:32:57.6	+26:52:45			0.18 ± 0.13	1.869	$5.0^{+2.3}_{-1.3}$	2500^{+2900}_{-1200}	3
1825500124644105728	IRAS 19312+1950	19:33:24.2	+19:56:57			0.42 ± 0.24	1.062	$2.8^{+1.5}_{-0.7}$	8000^{+11000}_{-4000}	2
2032744769234150016	IRAS 19327+3024	19:34:45.3	+30:30:57	W9	4.643	0.618 ± 0.032	0.9284	$1.562^{+0.068}_{-0.071}$	6210^{+560}_{-550}	3
2032364166432389760	IRAS 19343+2926	19:36:18.8	+29:32:49	B0	4.49	0.628 ± 0.093	1.606	$1.57^{+0.23}_{-0.19}$	2160^{+680}_{-480}	1
4301238979044890496	IRAS 19356+0754	19:38:01.2	+08:01:32			0.318 ± 0.094	2.418	$3.3^{+1.1}_{-0.8}$	780^{+630}_{-340}	1
2020388045260203008	IRAS 19374+2359	19:39:35.7	+24:06:28	B4	4.22	-1.16 ± 0.47	1.873	$5.2^{+2.4}_{-2.1}$	15000^{+17000}_{-10000}	1
2022052808961769088	IRAS 19376+2622	19:39:43.3	+26:29:35			0.5 ± 0.15	2.686	$2.5^{+1.1}_{-0.8}$	2900^{+3100}_{-1600}	3
4240112390324832384	IRAS 19386+0155	19:41:08.3	+02:02:30	F5Ib	3.81	0.32 ± 0.16	11.59	$3.6^{+2.0}_{-1.2}$	7000^{+10000}_{-4000}	1
4318934003785783680	IRAS 19396+1637	19:41:57.0	+16:44:39	M7	3.47	0.97 ± 0.1	5.74	$1.04^{+0.12}_{-0.10}$	1930^{+470}_{-360}	3
2049034819957965312	IRAS 19410+3733	19:42:53.0	+37:40:42	F3Ib	3.83	1.042 ± 0.02	1.082	$0.945^{+0.019}_{-0.024}$	1016^{+41}_{-51}	2
2031794791233840128	IRAS 19454+2920	19:47:24.8	+29:28:11	A0	3.99	0.098 ± 0.025	1.048	$6.8^{+1.3}_{-0.9}$	18300^{+7800}_{-4700}	1
2033763428091006720	IRAS 19475+3119	19:49:29.4	+31:27:16	F3Ibe	3.83	0.316 ± 0.021	1.429	$2.97^{+0.16}_{-0.18}$	22300^{+2500}_{-2700}	1
2020571869841643392	IRAS 19477+2401	19:49:55.0	+24:08:55	F5I	3.81	0.56 ± 0.62	2.321	$4.1^{+2.1}_{-1.9}$	4300^{+5400}_{-3100}	1

Table 1 (continued).

Gaia DR3 source id	SIMBAD name	RA h:m:s	DEC deg:m:s	SpType	$T_{\rm eff}$ log([K])	Parallax [mas]	RUWE	Distance [kpc]	Luminosity [$L_\odot$]	Vickers category
2026709201998745472	IRAS 19480+2504	19:50:08.3	+25:11:59	C-rich		0.7 ± 0.34	1.006	$3.4^{+2.3}_{-1.7}$	4700^{+8500}_{-3600}	1
6871175064823382912	IRAS 19500-1709	19:52:52.7	-17:01:49	F4Ia	3.82	0.399 ± 0.031	1.009	$2.31^{+0.17}_{-0.14}$	5460^{+840}_{-660}	1
2074302426124470656	IRAS 19589+4020	20:00:42.9	+40:29:09	F5I	3.81	-0.47 ± 0.16	10.96	$10.0^{+4.4}_{-3.0}$	5200^{+5600}_{-2700}	1
6879196723703009920	IRAS 19590-1249	20:01:49.9	-12:41:17	B1Ibe	4.42	0.152 ± 0.026	0.9832	$4.73^{+0.68}_{-0.58}$	1750^{+540}_{-400}	1
2034134414507432064	IRAS 20000+3239	20:01:59.5	+32:47:32	G2I	3.73	0.205 ± 0.049	2.246	$4.6^{+1.5}_{-0.9}$	10300^{+7800}_{-3600}	1
2030200671149815424	IRAS 20004+2955	20:02:27.2	+30:04:25	G7Ia	3.67	0.239 ± 0.018	0.9075	$3.72^{+0.26}_{-0.24}$	52200^{+7700}_{-6400}	1
4190636669164572928	IRAS 20023-1144	20:05:05.3	-11:35:58	F2II	3.85	1.336 ± 0.027	0.8088	$0.727^{+0.016}_{-0.013}$	1763^{+76}_{-64}	2
2055174630333744384	IRAS 20042+3259	20:06:10.6	+33:07:51			0.409 ± 0.037	1.179	$2.29^{+0.20}_{-0.19}$	110^{+20}_{-17}	1
2060806470651334912	IRAS 20094+3721	20:11:16.6	+37:30:52			0.53 ± 0.011	1.029	$1.787^{+0.038}_{-0.041}$	1412^{+61}_{-64}	2
1803364717856260736	IRAS 20136+1309	20:16:00.6	+13:18:56	F5I	3.81	0.279 ± 0.074	4.92	$3.7^{+1.6}_{-0.8}$	1000^{+1000}_{-400}	1
2060616220769708672	IRAS 20145+3656	20:16:26.3	+37:06:09	B	4.26	-0.15 ± 0.074	3.182	$9.4^{+2.6}_{-1.8}$	60000^{+37000}_{-20000}	3
1836195688380634368	IRAS 20160+2734	20:18:05.9	+27:44:04	F3Ie	3.83	0.391 ± 0.016	1.041	$2.317^{+0.093}_{-0.080}$	4080^{+330}_{-280}	1
2054521833963867008	IRAS 20174+3222	20:19:27.9	+32:32:16			0.124 ± 0.044	1.365	$5.2^{+1.4}_{-0.9}$	2100^{+1200}_{-600}	1
2056435602670418688	IRAS 20244+3509	20:26:25.0	+35:19:13			0.528 ± 0.026	1.144	$1.694^{+0.074}_{-0.063}$	299^{+26}_{-22}	2
1859190569633451648	IRAS 20406+2953	20:42:45.9	+30:04:08			0.21 ± 0.12	2.219	$3.9^{+1.4}_{-0.9}$	4600^{+3900}_{-1900}	3
1869422453048750336	IRAS 20462+3416	20:48:16.6	+34:27:23	B1	4.42	0.172 ± 0.018	1.235	$4.72^{+0.35}_{-0.37}$	4410^{+670}_{-660}	1
2193902559325301760	IRAS 20490+5934	20:50:13.4	+59:45:50	A3e	3.95	2.062 ± 0.016	0.8655	$0.4819^{+0.0035}_{-0.0037}$	$151.4^{+2.2}_{-2.3}$	2
2197298400984984064	IRAS 20559+6416	20:56:53.5	+64:28:32			2.241 ± 0.029	1.813	$0.4394^{+0.0058}_{-0.0063}$	$50.0^{+1.3}_{-1.4}$	2
1731164844433296128	IRAS 20547+0247	20:57:16.3	+02:58:43			0.189 ± 0.054	3.259	$4.8^{+1.1}_{-0.9}$	12300^{+6200}_{-4300}	2
2168803045330976768	IRAS 20572+4919	20:58:55.6	+49:31:15	F3Ie	3.83	1.577 ± 0.012	0.9983	$0.6230^{+0.0052}_{-0.0038}$	$118.4^{+2.0}_{-1.5}$	2
2179471159976791168	IRAS 21289+5815	21:30:22.8	+58:28:52	A9	3.88	1.011 ± 0.02	1.362	$0.964^{+0.017}_{-0.017}$	$22.33^{+0.78}_{-0.77}$	2
6831062200578042624	PHL 1580	21:30:25.2	-19:22:33			3.156 ± 0.018	0.9539	$0.3142^{+0.0016}_{-0.0015}$	$2.369^{+0.024}_{-0.022}$	1
6616993471402951680	BPS CS29493-0046	21:50:05.8	-30:49:11	B	4.26	0.05 ± 0.04	0.9237	$14.8^{+4.6}_{-6.5}$	620^{+440}_{-420}	2
6824212243136821248	PHL 174	21:50:48.6	-19:42:00	B3	4.26	0.063 ± 0.035	1.022	$8.4^{+2.0}_{-1.7}$	600^{+320}_{-210}	1
1976077657917533952	IRAS 21546+4721	21:56:33.1	+47:36:13			0.028 ± 0.028	1.818	$9.8^{+1.8}_{-1.5}$	2010^{+800}_{-580}	1
2005246464463628800	IRAS 22023+5249	22:04:12.2	+53:03:59	B1	4.42	0.173 ± 0.018	1.22	$5.28^{+0.58}_{-0.48}$	4300^{+1000}_{-700}	1
1958757291756223104	IRAS 22223+4327	22:24:31.3	+43:43:12	F7I	3.79	0.332 ± 0.026	1.685	$2.68^{+0.20}_{-0.13}$	2340^{+360}_{-220}	1
2006425553228658816	IRAS 22272+5435	22:29:10.4	+54:51:07	G5Ia	3.7	0.686 ± 0.028	1.184	$1.410^{+0.055}_{-0.054}$	6170^{+490}_{-460}	1
2594762641717531008	IRAS 22327-1731	22:35:27.5	-17:15:26	A0III	3.99	1.385 ± 0.056	2.313	$0.702^{+0.028}_{-0.022}$	182^{+15}_{-11}	1
6385794694664872320	CD-68 2300	22:40:48.1	-67:41:18	B8	4.06	0.704 ± 0.022	0.9883	$1.390^{+0.049}_{-0.046}$	2470^{+180}_{-160}	2
1932229409071269248	BD+39 4926	22:46:11.2	+40:06:26	B8	4.06	0.18 ± 0.037	2.188	$4.8^{+1.0}_{-0.7}$	4000^{+1800}_{-1200}	1
2015785313459952128	IRAS 23304+6147	23:32:44.7	+62:03:51	G2Ia	3.73	0.237 ± 0.028	1.586	$3.98^{+0.41}_{-0.36}$	5200^{+1100}_{-900}	1